NIST Author Manuscript

NIST Author Manuscript

NIST Author Manuscript

Author Manuscript

Accepted for publication in a peer-reviewed journal

NIST National Institute of Standards and Technology • U.S. Department of Commerce

Published in final edited form as:

J Am Chem Soc. 2019 March 06; 141(9): 4130–4136. doi:10.1021/jacs.9b00232.

Pore Space Partition within a Metal−Organic Framework for Highly Efficient C_2H_2/CO_2 Separation

Yingxiang Ye[†,‡], **Zhenlin Ma**[†], **Rui-Biao Lin**[‡], **Rajamani Krishna**[§], **Wei Zhou**[‖], **Quanjie Lin**[†], **Zhangjing Zhang**[*,†], **Shengchang Xiang**[*,†], **Banglin Chen**[*,‡]

[†]Fujian Provincial Key Laboratory of Polymer Materials, College of Chemistry and Materials Science, Fujian Normal University, 32 Shangsan Road, Fuzhou 350007, PR China

[‡]Department of Chemistry, University of Texas at San Antonio, One UTSA Circle, San Antonio, Texas 78249-0698, United States

[§]Van't Hoff Institute for Molecular Sciences, University of Amsterdam, Science Park 904, 1098 XH Amsterdam, The Netherlands

[‖]Center for Neutron Research, National Institute of Standards and Technology, Gaithersburg, Maryland 20899-6102, United States

Abstract

The pore space partition (PSP) approach has been employed to realize a novel porous MOF (**FJU-90**) with dual functionalities for the challenging C_2H_2/CO_2 separation under ambient conditions. By virtue of a triangular ligand (Tripp = 2,4,6-tris(4-pyridyl)pyridine), the cylindrical channels in the original **FJU-88** have been partitioned into uniformly interconnected pore cavities, leading to the dramatically reduced pore apertures from 12.0 × 9.4 to 5.4 × 5.1 $Å^2$. Narrowing down the pore sizes, the resulting activated **FJU-90a** takes up a very large amount of C_2H_2 (180 $cm^3\ g^{-1}$) but much less of CO_2 (103 $cm^3\ g^{-1}$) at 298 K and 1 bar, demonstrating it to be the best porous MOF material for this C_2H_2/CO_2 (50%:50%) separation in terms of the C_2H_2 gravimetric productivity. IAST calculations, molecular modeling studies, and simulated and experimental breakthrough experiments comprehensively demonstrate that the pore space partition strategy is a very powerful approach to constructing MOFs with dual functionality for challenging gas separation.

[*]**Corresponding Authors** zzhang@fjnu.edu.cn, scxiang@fjnu.edu.cn, banglin.chen@utsa.edu.

ASSOCIATED CONTENT

Supporting Information

The Supporting Information is available free of charge on the ACS Publications website at DOI: 10.1021/jacs.9b00232.

Additional structural figures, FTIR spectrum, TGA curves, PXRD patterns, gas adsorption isotherms, and breakthrough curves (DOCX)

FJU-90 (CIF)

The authors declare no competing financial interest.

NIST Author Manuscript NIST Author Manuscript NIST Author Manuscript

INTRODUCTION

Porous metal−organic frameworks (MOFs) have emerged as very promising materials for gas separation and purification because of their tunable pore sizes in reach sieving effects and their functional pore surfaces in directing the preferential binding of one gas molecule over another.[1−8] Over the past two decades, a large number of porous MOFs have been realized for different gas separation and purification schemes, ranging from comparatively less challenging ones such as CO_2/N_2 and CO_2/CH_4[9,10] to more challenging ones such as alkyne/alkene and olefin/paraffin separation.[11−18] Because C_2H_2 and CO_2 gas molecules have very similar physical properties (boiling points: C_2H_2, 189.3 K; CO_2, 194.7 K; molecular shapes and sizes: C_2H_2, 3.3 × 3.3 × 5.7 $Å^3$; CO_2, 3.2 × 3.3 × 5.4 $Å^3$)[19] and almost identical kinetic diameters of ~3.3 Å, it is very difficult and challenging to realize the porous materials for C_2H_2/CO_2. The first porous MOF or porous coordination polymer for this separation was realized back in 2005 in which the oxygen basic sites play important roles in inducing their stronger interactions with acetylene molecules.[20] It took quite a long time for the community to target a few porous MOFs for this separation at room temperature.[21−26] The unique UTSA-74,[21] the MOF-Zn-74 isomer, takes up much more acetylene over carbon dioxide under low pressures of up to 1 bar attributed to the accessible Zn^{2+} binding two acetylene molecules but only one carbon dioxide gas molecules, unlike MOF-Zn-74 which adsorbs similar amounts of acetylene and carbon dioxide under 1 bar. Another porous MOF for this separation is a flexible MOF, UTSA-300a,[23] in which the acetylene molecule can trigger a structural change and thus can open the pores through the C−H···F hydrogen bonding interactions. The acetylene uptake in UTSA-300a is accordingly not very high at about 69 cm^3/g under ambient conditions.

The ideal porous materials for gas separation/purification are those with both high gas uptake and separation selectivities, posing daunting challenges for scientists and engineers, a so-called trade-off. We have made some progress over the past several years in addressing these challenges through so-called dual functionalities in which both pore sizes and functional surfaces simultaneously enforce gas separations without the sacrifice of moderate pore volumes or surface areas to take up large numbers of the preferred gas molecules. Although such a dual-functionality approach is quite efficient in realizing porous MOFs for gas separations, the porous MOFs, UTSA-16 for CO_2/N_2 separation and UTSA-100 for C_2H_2/C_2H_4 separation,[27,28] respectively, were basically discovered unexpectedly without any rational design. In this regard, the approach developed by Bu and Feng, termed the pore space partition (PSP),[29−37] is particularly interesting and important. It means that the pore spaces in some porous MOFs with large pores can be rationally partialized. To further make use of the functional pore surfaces, such a PSP approach might provide us with a much more rational strategy for realizing novel porous MOFs with dual functionalities and thus for gas separation/purification.

Herein we report a rare example (termed **FJU-90**) of such MOFs through this PSP approach to C_2H_2/CO_2 separation. As shown in Figure 1 (left), the mother MOF, **FJU-88**,[38] has a very large one-dimensional pore space (pore sizes of about 10.1 × 10.1 $Å^2$ and 12.0 × 9.4 $Å^2$) which is not good for gas separation. Once the pore spaces were partialized through the immobilization of a C_3-symmetric 2,4,6-tris(4-pyridyl)pyridine (Tripp) regulated ligand, the

NIST Author Manuscript NIST Author Manuscript NIST Author Manuscript

pore spaces were rationally partialized to up to 9.5 Å with an aperture size of only 5.4 × 5.1 $Å^2$. The resulting activated **FJU-90a** takes up a very large amount of acetylene (180 cm^3 g^{-1}) but much less carbon dioxide (103 cm^3 g^{-1}) at 298 K and 1 bar, demonstrating it to be the best porous MOF material for this C_2H_2/CO_2 (50%:50%) separation in terms of the C_2H_2 gravimetric productivity. Molecular modeling studies and simulated and experimental breakthroughs have well supported the results in which both optimized pore sizes and pore surfaces of O atoms for the HC ≡ C – H···O hydrogen bonding interactions have collaborative roles in this very challenging gas separation.

EXPERIMENTAL SECTION

Materials and Physical Measurements.

All reagents and solvents were commercially available and directly used without further purification. Organic ligands 4-(4*H*-1,2,4-triazol-4-yl)benzoic acid (HCPT)[39] and 2,4,6-tris(4-pyridyl)pyridine (Tripp)[40] were synthesized according to the previously reported procedure. A PerkinElmer 240C elemental analyzer was used to obtain elemental analyses of C, H, and N. A Fourier-transform infrared spectrum (FTIR, KBr pellets) was recorded on a Thermo Nicolet 5700 FT-IR instrument from 4000 to 400 cm^{-1}. Thermogravimetric analysis (TGA) was carried out under an air atmosphere from room temperature to 600 °C using a Shimadzu TGA-50 analyzer at a heating rate of 5 °C min^{-1}. Powder X-ray diffraction (PXRD) patterns were recorded by a PANalytical X'Pert[3] powder diffractometer equipped with a Cu sealed tube (λ = 1.54184 Å) at 40 kV and 40 mA over the 2θ range of 5−40°. The simulated pattern was produced using the Mercury V1.4 program and single-crystal diffraction data.

Synthesis of FJU-88.

FJU-88 was previously synthesized.[38] A mixture of HCPT (94 mg, 0.5 mmol) and $CoCl_2 \cdot 6H_2O$ (120 mg, 0.5 mmol) was dissolved in a mixed solution of DMA-H_2O-HBF_4 (21 mL, 10:3:1 v/v/v) and then held in a 120 °C oven for 1 day. After cooling to room temperature, the light-orange rod-shaped single crystals were obtained (yield 65%, based on HCPT).

Synthesis of FJU-90.

A mixture of HCPT (94 mg, 0.5 mmol), Tripp (100 mg, 0.32 mmol), and $CoCl_2 \cdot 6H_2O$ (120 mg, 0.5 mmol) was dissolved in the mixed solution of DMA-H_2O-HBF_4 (21 mL, 10:3:1 v/v/v) and then held in a 120 °C oven for 1 day. After cooling to room temperature, the orange polyhedral-shaped crystals that formed were collected, washed with DMA, and dried in air (yield 62%, based on HCPT). Elemental analysis calculated (%) for [Co_3(μ_3-OH)(CPT)$_3$(Tri pp)]Cl_2(DMA)$_{5.5}$(H_2O)$_8$ - ($C_{69}H_{98.5}Co_3N_{18.5}O_{20.5}Cl_2$): C, 46.98; H, 5.59; N, 14.69. Found: C, 47.04; H, 5.72; N, 14.37.

Single-Crystal X-ray Diffraction (SCXRD) Studies.

Data collection and structural analysis of crystal **FJU-90** was collected on the Rigaku Oxford single-crystal diffractometer equipped with graphite monochromatic Cu Kα radiation (λ = 1.54184 Å). The crystal was kept at 150 K during data collection. Using

NIST Author Manuscript NIST Author Manuscript NIST Author Manuscript

Olex2,[41] the structure was solved with the Superflip[42] structure solution program using charge flipping and refined with the ShelXL[43] refinement package using least-squares minimization. The CPT ligand is disordered over two positions (occupancy 0.5:0.5); this is because the triazolate and carboxylate parts of the ligand show similar coordination models and therefore can substitute for each other at the given site. Additionally, the disorder of the triazolate group leads to the carbon and nitrogen atoms sharing the same crystallographic positions with partial occupancies. All nonhydrogen atoms were refined with anisotropic displacement parameters. The hydrogen atoms on the ligands were placed in idealized positions and refined using a riding model. We employed PLATON[44] and SQUEEZE[45] to calculate the diffraction contribution of the solvent molecules and thereby produce a set of solvent-free diffraction intensities. The detailed crystallographic data and structure refinement parameters are summarized in Table S2 (CCDC 1882901).

Gas Adsorption Measurements.

To remove all of the guest solvents in the framework, a fresh sample of **FJU-88** or **FJU-90** (~150 mg) was guest-exchanged with dry CH_3OH at least 10 times, filtered, and degassed at 60 °C until the outgas rate was 5 μmHg min^{-1} prior to measurements. C_2H_2, CO_2, and N_2 adsorption isotherms were measured on Micromeritics ASAP 2020 HD88 surface area analyzer for the guest-free sample. An ice−water bath (slush) and a water bath were used for adsorption isotherms at 273 and 298 K, respectively. Pore size distribution (PSD) data was obtained from the 273 K CO_2 and 77 K N_2 adsorption isotherms based on the nonlocal density functional theory (NLDFT) model.[46]

Column Breakthrough Experiments.

The breakthrough experiments were carried out in a self-made dynamic mixed-gas breakthrough setup.[47,48] A stainless steel column with inner dimensions of $\phi = 4 \times 150$ mm was used for sample packing. A microcrystalline sample with a particle size of 220−320 μm obtained via sieving was then packed into the column. The mixed-gas flow and pressure were controlled by using a pressure-control valve and a mass flow controller. Outlet effluent from the column was continuously monitored using gas chromatography (GC-2014, Shimadzu) with a thermal conductivity detector (TCD). The column packed with sample was first purged with a flow of He (50 mL min^{-1}) for 1 h at room temperature. The mixed-gas flow rate during the breakthrough process is 2 mL min^{-1} using 50/50 (v/v) C_2H_2/CO_2 at room temperature (298 K). After the breakthrough experiment, the sample was regenerated under vacuum.

On the basis of the mass balance, the gas adsorption capacities can be determined as follows

$$q_i = \frac{C_i V}{22.4m} \int_0^t \left(1 - \frac{F}{F_0}\right) \mathrm{d}t \quad (1)$$

where q_i is the equilibrium adsorption capacity of gas i (mmol g^{-1}), C_i is the feed gas concentration, V is the volumetric feed flow rate (mL min^{-1}), t is the adsorption time (min),

NIST Author Manuscript NIST Author Manuscript NIST Author Manuscript

F_0 and F are the inlet and outlet gas molar flow rates, respectively, and m is the mass of the adsorbent (g).

RESULTS AND DISCUSSION

Solvothermal reaction of HCPT and Tripp with $CoCl_2 \cdot 6H_2O$ in the mixed DMA/H_2O solution at 120 °C for 1 day afforded orange polyhedral-shaped crystals of **FJU-90** (Figure S1). Single-crystal X-ray diffraction analysis revealed that **FJU-90** crystallizes in the hexagonal $P6_3/mmc$ space group, the same as for prototypical MOF **FJU-88**. It is noteworthy that the [$Co_3(\mu_3$-OH)] unit in **FJU-88** is a six-connected node, while the unit becomes nine-connected in **FJU-90** because the three axial positions were occupied by the pyridyl groups from the Tripp ligands (Figure 1a). Notably, compared with **FJU-88**, the PSP has resulted in a significant decrease in the window size of the trigonal bipyramidal cage from 12.0 × 9.4 $Å^2$ to 5.4 × 5.1 $Å^2$ (taking into account the van der Waals radii of the atoms, Figure S2). Simultaneously, the original 1D cylindrical channel along the crystallographic c axis (with an aperture size of 10.1 × 10.1 $Å^2$) has been divided by the Tripp partitions (at an interval of ca. 9.5 Å) into numerous uniform interconnected pore cavities, which displays the potential for enhanced confinement effects and multiple-point adsorption (dual functionalities), especially for C_2H_2 with acidic H atoms (Figure 1b).[49] Topologically, if the Tripp ligand and the [$Co_3(\mu_3$-OH)] unit are simplified as 3- and 9-c nodes, respectively, then the 3D framework of **FJU-90** exhibits a (3,9)-connected network with a point symbol of $(4^3)(4^{21}6^{15})$ (**nia-d** topology),[50] which is notably rigid as compared to the original 6-c network (**acs** topology, Figure 1c). Without considering the guest solvent molecules, the total accessible volumes in **FJU-90** are estimated to be 62%, slightly lower than for the prototypical structure (72%), as calculated by PLATON software, which is reasonable considering the space occupancy of Tripp ligands. Obviously, the pore volume after the pore space partition approach is still higher than those of many other highly selective MOF adsorbents.[11,16,51]

The phase purities of the prepared bulk products were verified by a comparison of the experimental and simulated powder X-ray diffraction (PXRD) patterns and further confirmed by thermogravimetric analysis and elemental analysis (Figures S6, S7, and S9). Notably, the thermal stability of **FJU-90** (up to 300 °C) is significantly higher than for original **FJU-88** (stable only below 50 °C), as proven by the variable-temperature PXRD experiments (Figures S8 and S12). Furthermore, the PXRD result further confirmed that the structure of **FJU-90** could be maintained after exposure to air for a month or soaking in water for 1 day, while **FJU-88** is unstable after soaking in water for 10 min (Figures S7 and S11). To explore the permanent porosity, the two MOF samples were guest-exchanged with anhydrous CH_3OH at least 10 times and then degassed at 60 °C under high vacuum to yield guest-free phases **FJU-88a** and **FJU-90a**. The PXRD pattern of **FJU-90a** revealed that the structural integrity was fully preserved after activation, while **FJU-88a** loses its crystallinity, which further proves that the host framework after the insertion of the Tripp ligand is more robust and stable than the original one (Figures S7 and S9, details in the Supporting Information).

NIST Author Manuscript NIST Author Manuscript NIST Author Manuscript

As shown in Figure 2, the 77 K N_2 adsorption isotherms of **FJU-90a** show fully reversible type-I behavior with a maximum N_2 uptake of 420 $cm^3\ g^{-1}$ at 1 bar, while **FJU-88a** basically takes up no N_2, which is ascribed to the collapse of the porous structures after activation. The corresponding pore volume in **FJU-90a** is 0.65 $cm^3\ g^{-1}$, which is slighter lower than the theoretical value of 0.74 $cm^3\ g^{-1}$ (calculated from the crystal structure) due to the insufficient filling of N_2 on the irregular pore surfaces of **FJU-90a** (Figure S4) but still higher than those of many other MOF sieves for gas separation.[11,16,51] The Brunauer−Emmett−Teller (BET) surface area of **FJU-90a** is up to 1572 $m^2\ g^{-1}$ as calculated from the N_2 adsorption isotherms, which is comparable to that of CPM-233 (1320 $m^2\ g^{-1}$)[31] but higher than that of Co-MOF1-tpt (826 $m^2\ g^{-1}$)[52] in the same type MOFs. The pore-size distribution (PSD) of **FJU-90a** was analyzed by using the 273 K CO_2 and 77 K N_2 isotherms based on the NLDFT model, which show narrow pore cavity size distributions with centers at 5.8 and 8.6 Å (Figure S14), which are close to the cavity sizes determined from the crystal structure.

Next, we collected the gas sorption isotherms of C_2H_2 and CO_2 for **FJU-88a** and **FJU-90a** at 273 and 298 K under 1 bar (Figure 3a) to explore their abilities for gas adsorption and separation. Owing to the high porosity, suitable pore space, and potential O basic sites, remarkable C_2H_2 uptake was observed in **FJU-90a**, with the adsorbed amounts of 216 and 180 cm^3 (STP) g^{-1} at 273 and 298 K, and 1 bar, respectively, which are systematically higher than that of **FJU-88a** under similar conditions (Figure S13, details in the Supporting Information). Notably, the C_2H_2 uptake capacity in **FJU-90a** under ambient conditions is higher than those in many renowned MOFs with a high density of open metal sites, such as ZJU-60a (150 $cm^3\ g^{-1}$),[53] ZnMOF-74 (122 $cm^3\ g^{-1}$),[54] PCP-33 (122 $cm^3\ g^{-1}$),[55] and UTSA-74a (104 $cm^3\ g^{-1}$),[21] and slightly lower than those for MFM-188a (232 $cm^3\ g^{-1}$),[56] FJI-H8 (224 $cm^3\ g^{-1}$),[57] and HKUST-1 (201 $cm^3\ g^{-1}$).[58] However, what is noteworthy is that the CO_2 uptake value of 103 $cm^3\ g^{-1}$ in **FJU-90a** is remarkably lower than that of C_2H_2 under similar conditions.

To assess the adsorption enthalpies of C_2H_2 and CO_2 in **FJU-90a**, the coverage-dependent isosteric heat of adsorption (Q_{st}) was calculated with the adsorption isotherms at 273 and 298 K and fitted with the dual-Langmuir isotherm model. As shown in Figure S16, the obtained Q_{st} value for C_2H_2 (25.1 kJ mol^{-1}) is obviously higher than that for CO_2 (20.7 kJ mol^{-1}), indicative of the stronger affinity of **FJU-90a** toward C_2H_2. We note that the Q_{st} value of C_2H_2 in **FJU-90a** is notably lower than for some famous MOF materials with a high density of open metal or F sites, for example, HKUST-1 (39 kJ mol^{-1}),[59] FeMOF-74 (47.5 kJ mol^{-1}),[59] and SIFSIX-2-Cu-i (41.9 kJ mol^{-1}).[11] These data highlight that **FJU-90a** is a promising candidate for the separation of C_2H_2/CO_2 with a lower regeneration energy requirement for C_2H_2. In addition, to help understand the unique adsorption behavior of **FJU-90a** for C_2H_2 and CO_2, we implemented dispersion-corrected density-functional theory (DFT-D) calculations.[60] Our results show that overall the calculated static C_2H_2 and CO_2 binding strengths in **FJU-90a** are modest, <40 kJ mol^{-1} (Figure S17; in contrast, the reported static gas binding energies in some SIFSIX MOFs are >50 kJ mol^{-1}).[11,51] Comparing the two different gases in **FJU-90a**, the calculated C_2H_2 binding affinity is clearly stronger than that of CO_2 because of the larger electrostatic interactions (between

NIST Author Manuscript NIST Author Manuscript NIST Author Manuscript

the charge on the framework and the distributed charge on the gas molecule) and strong HC ≡ C – H···O hydrogen bonding interactions. This accounts for the higher Q_{st} and uptake capacity of C_2H_2 observed experimentally. Furthermore, the DFT-D calculations further demonstrated that the pore space partition approach is feasible for constructing MOFs featuring dual functionalities for separating the C_2H_2/CO_2 mixture.

To address C_2H_2/CO_2 mixture separations, the well-defined approach of the ideal adsorbed solution theory (IAST)[61] is employed to evaluate the adsorption selectivity and uptake capacity at different pressures. Figure 3b presents IAST calculations of the C_2H_2 uptake capacity as a function of the total gas pressure, and Figure S22 provides a comparison of the adsorption selectivity of the binary equimolar C_2H_2/CO_2 mixture in **FJU-90a** with those of the other four MOFs at 298 K. We note that the IAST selectivity of **FJU-90a** (4.3) is slightly lower than that of benchmark material UTSA-74a (8.2) and comparable to other famous MOFs, and more importantly, the C_2H_2 uptake value in **FJU-90a** is remarkably higher than those of other best-performing MOFs under 100 kPa.

To accurately assess the combined effects of the adsorption selectivity and uptake capacity, we performed the transient breakthrough simulations by using the previously reported simulation methodology.[62] As shown in Figure 3c, CO_2 eluted first, and this continued for a remarkable time until C_2H_2 broke through as its saturated uptake in **FJU-90a**. Therefore, the simulation results demonstrate that **FJU-90a** is one of the promising candidates for addressing the challenge of C_2H_2/CO_2 mixture separation.

Furthermore, Figure 3d displays a comparison of C_2H_2 captured productivity (mol kg^{-1}, based on the simulated column breakthrough) for **FJU-90a** with other best-performing MOFs (including UTSA-74a,[21] FJU-22a,[63] PCP-33,[55] Zn-MOF-74,[54] and ZJU-60a[53]). It was worth noting that the separation performance (selectivity and productivity) for C_2H_2/CO_2 mixtures in **FJU-90a** is systematically higher than that of ZnMOF-74. The C_2H_2 volumetric productivity in **FJU-90a** (4.16 mol L^{-1}) is slightly lower than for benchmark material UTSA-74a (4.86 mol L^{-1}); however, **FJU-90a** exhibits the highest gravimetric productivity with a value of 5.10 mol kg^{-1}, which is much higher than for UTSA-74a (3.47 mol kg^{-1}). Therefore, the outstanding C_2H_2/CO_2 separation performance of **FJU-90a** should be attributed to the combination of high C_2H_2 uptake capacity and moderate adsorption selectivity.

Acetylene (C_2H_2) is an essential chemical feedstock for modern petrochemical products such as acrylic acid derivatives, vinyl chloride, plastics, and rubber.[64] However, CO_2 as an impurity always exists in the production process of acetylene. To further evaluate the actual separation performance of the C_2H_2/CO_2 mixture in **FJU-90a**, we carried out laboratory-scale fixed-bed breakthrough experiments under ambient conditions in which the C_2H_2/CO_2 (50/50) gas mixture flowed over a packed column at a total flow rate of 2 mL min^{-1}. Figure 4a shows that **FJU-90a** can achieve a highly efficient separation of C_2H_2/CO_2 mixtures. CO_2 was first eluted and then quickly approached a pure grade without detectable C_2H_2, whereas C_2H_2 was retained in the packed column for a remarkable time until its saturated uptake and breakthrough. The dynamic C_2H_2 capture productivity, calculated on the basis of the breakthrough curve, was found to be 1.87 mol kg^{-1}. For practical industrial applications,

NIST Author Manuscript NIST Author Manuscript NIST Author Manuscript

the ideal adsorbent should have good recyclability. Thus, we implemented five C_2H_2/CO_2 dynamic breakthrough experiments under the current operating conditions, and the results showed that FJU-90a maintained the same retention time and acetylene uptake capacity as the initial one (Figure 4b). Further investigations of **FJU-90a** with larger gas flow or ultralow gas concentration also showed outstanding separation performance for challenging C_2H_2/CO_2 mixtures. Moreover, **FJU-90a** retained its stability after the breakthrough cycling test (Figures S23−S26, details in the Supporting Information).

In summary, we have successfully realized a microporous MOF (**FJU-90**) with dual functionality for highly selective C_2H_2/CO_2 separation through the pore space partition (PSP) strategy. The partitioning of the tripyridine ligands not only improves the framework stability but also reduces the pore aperture sizes for the enhanced sieving effect for gas separation. Notably, **FJU-90a** exhibits both a moderately high C_2H_2 uptake capacity and adsorption selectivity, affording new benchmark C_2H_2 captured productivity with respect to C_2H_2/CO_2 (50%:50%) separation under ambient conditions. This work represents an outstanding example of the PSP strategy for rationally designing microporous MOF materials for challenging gas separation/purification, thus significantly facilitating this very active ongoing research.

Supplementary Material

Refer to Web version on PubMed Central for supplementary material.

ACKNOWLEDGMENTS

This work was financially supported by the National Natural Science Foundation of China (21673039, 21573042, and 21273033), the Fujian Science and Technology Department (2018J07001, 2016J01046, and 2014J06003) and the Welch Foundation (AX-1730). Y.Y. gratefully acknowledges the support of the China Scholarship Council.

REFERENCES

(1). Furukawa H; Cordova KE; O'Keeffe M; Yaghi OM The Chemistry and Applications of Metal-Organic Frameworks. Science 2013, 341, 1230444.

(2). Li JR; Kuppler RJ; Zhou HC Selective gas adsorption and separation in metal-organic frameworks. Chem. Soc. Rev. 2009, 38, 1477. [PubMed: 19384449]

(3). Bao Z; Chang G; Xing H; Krishna R; Ren Q; Chen B. Potential of microporous metal−organic frameworks for separation of hydrocarbon mixtures. Energy Environ. Sci. 2016, 9, 3612.

(4). Zhao X; Wang Y; Li D-S; Bu X; Feng P. Metal−Organic Frameworks for Separation. Adv. Mater. 2018, 30, 1705189.

(5). Cui Y; Li B; He H; Zhou W; Chen B; Qian G. Metal−Organic Frameworks as Platforms for Functional Materials. Acc. Chem. Res. 2016, 49, 483. [PubMed: 26878085]

(6). Cui Y; Yue Y; Qian G; Chen B. Luminescent Functional Metal−Organic Frameworks. Chem. Rev. 2012, 112, 1126. [PubMed: 21688849]

(7). Wang H; Dong X; Velasco E; Olson DH; Han Y; Li J. One-of-a-kind: a microporous metal−organic framework capable of adsorptive separation of linear, mono- and di-branched alkane isomers via temperature- and adsorbate-dependent molecular sieving. Energy Environ. Sci. 2018, 11, 1226.

(8). Vaidhyanathan R; Iremonger SS; Shimizu GKH; Boyd PG; Alavi S; Woo TK Direct Observation and Quantification of CO_2 Binding Within an Amine-Functionalized Nanoporous Solid. Science 2010, 330, 650. [PubMed: 21030651]

NIST Author Manuscript NIST Author Manuscript NIST Author Manuscript

(9). Adil K; Bhatt PM; Belmabkhout Y; Abtab SMT; Jiang H; Assen AH; Mallick A; Cadiau A; Aqil J; Eddaoudi M. Valuing Metal-Organic Frameworks for Postcombustion Carbon Capture: A Benchmark Study for Evaluating Physical Adsorbents. Adv. Mater. 2017, 29, 1702953.

(10). Belmabkhout Y; Bhatt PM; Adil K; Pillai RS; Cadiau A; Shkurenko A; Maurin G; Liu G; Koros WJ; Eddaoudi M. Natural gas upgrading using a fluorinated MOF with tuned H_2S and CO_2 adsorption selectivity. Nature Energy 2018, 3, 1059.

(11). Cui X; Chen K; Xing H; Yang Q; Krishna R; Bao Z; Wu H; Zhou W; Dong X; Han Y; Li B; Ren Q; Zaworotko MJ; Chen B. Pore chemistry and size control in hybrid porous materials for acetylene capture from ethylene. Science 2016, 353, 141. [PubMed: 27198674]

(12). Li L; Lin R-B; Krishna R; Li H; Xiang S; Wu H; Li J; Zhou W; Chen B. Ethane/ethylene separation in a metal-organic framework with iron-peroxo sites. Science 2018, 362, 443. [PubMed: 30361370]

(13). Lin RB; Li L; Zhou HL; Wu H; He C; Li S; Krishna R; Li J; Zhou W; Chen B. Molecular sieving of ethylene from ethane using a rigid metal-organic framework. Nat. Mater. 2018, 17, 1128. [PubMed: 30397312]

(14). Bloch ED; Queen WL; Krishna R; Zadrozny JM; Brown CM; Long JR Hydrocarbon Separations in a Metal-Organic Framework with Open Iron(II) Coordination Sites. Science 2012, 335, 1606. [PubMed: 22461607]

(15). Wang H; Dong X; Colombo V; Wang Q; Liu Y; Liu W; Wang X-L; Huang X-Y; Proserpio DM; Sironi A; Han Y; Li J. Tailor-Made Microporous Metal−Organic Frameworks for the Full Separation of Propane from Propylene Through Selective Size Exclusion. Adv. Mater. 2018, 30, 1805088.

(16). Cadiau A; Adil K; Bhatt PM; Belmabkhout Y; Eddaoudi M. A metal-organic framework−based splitter for separating propylene from propane. Science 2016, 353, 137. [PubMed: 27387945]

(17). Liao P-Q; Huang N-Y; Zhang W-X; Zhang J-P; Chen X-M Controlling guest conformation for efficient purification of butadiene. Science 2017, 356, 1193. [PubMed: 28619946]

(18). Liao P-Q; Zhang W-X; Zhang J-P; Chen X-M Efficient purification of ethene by an ethane-trapping metal-organic framework. Nat. Commun. 2015, 6, 8697. [PubMed: 26510376]

(19). Reid CR; Thomas KM Adsorption Kinetics and Size Exclusion Properties of Probe Molecules for the Selective Porosity in a Carbon Molecular Sieve Used for Air Separation. J. Phys. Chem. B 2001, 105, 10619.

(20). Matsuda R; Kitaura R; Kitagawa S; Kubota Y; Belosludov RV; Kobayashi TC; Sakamoto H; Chiba T; Takata M; Kawazoe Y; Mita Y. Highly controlled acetylene accommodation in a metal−organic microporous material. Nature 2005, 436, 238. [PubMed: 16015325]

(21). Luo F; Yan C; Dang L; Krishna R; Zhou W; Wu H; Dong X; Han Y; Hu TL; O'Keeffe M; Wang L; Luo M; Lin RB; Chen B. UTSA-74: A MOF-74 Isomer with Two Accessible Binding Sites per Metal Center for Highly Selective Gas Separation. J. Am. Chem. Soc. 2016, 138, 5678. [PubMed: 27113684]

(22). Chen K-J; Scott HS; Madden DG; Pham T; Kumar A; Bajpai A; Lusi M; Forrest KA; Space B; Perry JJ; Zaworotko MJ Benchmark C_2H_2/CO_2 and CO_2/C_2H_2 Separation by Two Closely Related Hybrid Ultramicroporous Materials. Chem. 2016, 1, 753.

(23). Lin RB; Li L; Wu H; Arman H; Li B; Lin RG; Zhou W; Chen B. Optimized Separation of Acetylene from Carbon Dioxide and Ethylene in a Microporous Material. J. Am. Chem. Soc. 2017, 139, 8022. [PubMed: 28574717]

(24). Lee J; Chuah CY; Kim J; Kim Y; Ko N; Seo Y; Kim K; Bae TH; Lee E. Separation of Acetylene from Carbon Dioxide and Ethylene by a Water-Stable Microporous Metal−Organic Framework with Aligned Imidazolium Groups inside the Channels. Angew. Chem., Int. Ed. 2018, 57, 7869.

(25). Peng Y-L; Pham T; Li P; Wang T; Chen Y; Chen K-J; Forrest KA; Space B; Cheng P; Zaworotko MJ; Zhang Z. Robust Ultramicroporous Metal−Organic Frameworks with Benchmark Affinity for Acetylene. Angew. Chem., Int. Ed. 2018, 57, 10971.

(26). Li L; Wang J; Zhang Z; Yang Q; Yang Y; Su B; Bao Z; Ren Q. Inverse Adsorption Separation of CO_2/C_2H_2 Mixture in Cyclodextrin-Based Metal−Organic Frameworks. ACS Appl. Mater. Interfaces 2019, 11, 2543. [PubMed: 30565914]

NIST Author Manuscript NIST Author Manuscript NIST Author Manuscript

(27). Xiang S; He Y; Zhang Z; Wu H; Zhou W; Krishna R; Chen B. Microporous metal-organic framework with potential for carbon dioxide capture at ambient conditions. Nat. Commun. 2012, 3, 954. [PubMed: 22805561]

(28). Hu T-L; Wang H; Li B; Krishna R; Wu H; Zhou W; Zhao Y; Han Y; Wang X; Zhu W; Yao Z; Xiang S; Chen B. Microporous metal−organic framework with dual functionalities for highly efficient removal of acetylene from ethylene/acetylene mixtures. Nat. Commun. 2015, 6, 7328. [PubMed: 26041691]

(29). Zhao X; Bu X; Zhai Q-G; Tran H; Feng P. Pore Space Partition by Symmetry-Matching Regulated Ligand Insertion and Dramatic Tuning on Carbon Dioxide Uptake. J. Am. Chem. Soc. 2015, 137, 1396. [PubMed: 25621414]

(30). Zhao X; Bu X; Nguyen ET; Zhai Q-G; Mao C; Feng P. Multivariable Modular Design of Pore Space Partition. J. Am. Chem. Soc. 2016, 138, 15102. [PubMed: 27933883]

(31). Zhai QG; Bu X; Mao C; Zhao X; Daemen L; Cheng Y; Ramirez-Cuesta AJ; Feng P. An ultra-tunable platform for molecular engineering of high-performance crystalline porous materials. Nat. Commun. 2016, 7, 13645. [PubMed: 27924818]

(32). Zhai QG; Bu X; Zhao X; Li DS; Feng P. Pore Space Partition in Metal-Organic Frameworks. Acc. Chem. Res. 2017, 50, 407. [PubMed: 28106984]

(33). Wei YS; Zhang M; Liao PQ; Lin RB; Li TY; Shao G; Zhang JP; Chen XM Coordination templated [2 + 2+2] cyclotrimerization in a porous coordination framework. Nat. Commun. 2015, 6, 8348. [PubMed: 26384254]

(34). Hong X-J; Wei Q; Cai Y-P; Wu B.-b.; Feng H-X; Yu Y; Dong R-F Pillar-Layered Metal−Organic Framework with Sieving Effect and Pore Space Partition for Effective Separation of Mixed Gas C_2H_2/C_2H_4. ACS Appl. Mater. Interfaces 2017, 9, 29374. [PubMed: 28792198]

(35). Lu Z; Zhang J; Duan J; Du L; Hang C. Pore space partition via secondary metal ions entrapped by pyrimidine hooks: influences on structural flexibility and carbon dioxide capture. J. Mater. Chem. A 2017, 5, 17287.

(36). Zhang H-X; Liu M; Xu G; Liu L; Zhang J. Selectivity of CO_2 via pore space partition in zeolitic boron imidazolate frameworks. Chem. Commun. 2016, 52, 3552.

(37). Chen D-M; Sun C-X; Zhang N-N; Si H-H; Liu C-S; Du M. Tunable Robust pacs-MOFs: a Platform for Systematic Enhancement of the C_2H_2 Uptake and C_2H_2/C_2H_4 Separation Performance. Inorg. Chem. 2018, 57, 2883. [PubMed: 29470067]

(38). Ye Y; Chen S; Chen L; Huang J; Ma Z; Li Z; Yao Z; Zhang J; Zhang Z; Xiang S. Additive-Induced Supramolecular Isomerism and Enhancement of Robustness in Co(II)-Based MOFs for Efficiently Trapping Acetylene from Acetylene-Containing Mixtures. ACS Appl. Mater. Interfaces 2018, 10, 30912. [PubMed: 30124288]

(39). Ye Y; Xiong S; Wu X; Zhang L; Li Z; Wang L; Ma X; Chen QH; Zhang Z; Xiang S. Microporous Metal-Organic Framework Stabilized by Balanced Multiple Host-Couteranion Hydrogen-Bonding Interactions for High-Density CO_2 Capture at Ambient Conditions. Inorg. Chem. 2016, 55, 292. [PubMed: 26653758]

(40). Smith CB; Raston CL; Sobolev AN Poly(ethyleneglycol) (PEG): a versatile reaction medium in gaining access to 4′-(pyridyl)-terpyridines. Green Chem. 2005, 7, 650.

(41). Dolomanov OV; Bourhis LJ; Gildea RJ; Howard JAK; Puschmann H. OLEX2: a complete structure solution, refinement and analysis program. J. Appl. Crystallogr. 2009, 42, 339.

(42). Palatinus L; Chapuis G. SUPERFLIP - a computer program for the solution of crystal structures by charge flipping in arbitrary dimensions. J. Appl. Crystallogr. 2007, 40, 786.

(43). Sheldrick G. A short history of SHELX. Acta Crystallogr., Sect. A: Found. Crystallogr. 2008, 64, 112.

(44). Spek A. Single-crystal structure validation with the program PLATON. J. Appl. Crystallogr. 2003, 36, 7.

(45). Sarkisov L; Harrison A. Computational structure characterisation tools in application to ordered and disordered porous materials. Mol. Simul. 2011, 37, 1248.

(46). Zhu Y; Murali S; Stoller MD; Ganesh KJ; Cai W; Ferreira PJ; Pirkle A; Wallace RM; Cychosz KA; Thommes M; Su D; Stach EA; Ruoff RS Carbon-Based Supercapacitors Produced by Activation of Graphene. Science 2011, 332, 1537. [PubMed: 21566159]

NIST Author Manuscript NIST Author Manuscript NIST Author Manuscript

(47). Lin R-B; Wu H; Li L; Tang X-L; Li Z; Gao J; Cui H; Zhou W; Chen B. Boosting Ethane/Ethylene Separation within Isoreticular Ultramicroporous Metal−Organic Frameworks. J. Am. Chem. Soc. 2018, 140, 12940. [PubMed: 30216725]

(48). Li L; Lin R-B; Krishna R; Wang X; Li B; Wu H; Li J; Zhou W; Chen B. Flexible−Robust Metal−Organic Framework for Efficient Removal of Propyne from Propylene. J. Am. Chem. Soc. 2017, 139, 7733. [PubMed: 28580788]

(49). Ma Y; Matsuda R; Sato H; Hijikata Y; Li L; Kusaka S; Foo M; Xue F; Akiyama G; Yuan R; Kitagawa S. A Convenient Strategy for Designing a Soft Nanospace: An Atomic Exchange in a Ligand with Isostructural Frameworks. J. Am. Chem. Soc. 2015, 137, 15825. [PubMed: 26592095]

(50). Chen D-M; Zhang N-N; Tian J-Y; Liu C-S; Du M. Pore modulation of metal−organic frameworks towards enhanced hydrothermal stability and acetylene uptake via incorporation of different functional brackets. J. Mater. Chem. A 2017, 5, 4861.

(51). Li B; Cui X; O'Nolan D; Wen HM; Jiang M; Krishna R; Wu H; Lin RB; Chen YS; Yuan D; Xing H; Zhou W; Ren Q; Qian G; Zaworotko MJ; Chen B. An Ideal Molecular Sieve for Acetylene Removal from Ethylene with Record Selectivity and Productivity. Adv. Mater. 2017, 29, 1704210.

(52). Gao Q; Zhao XL; Chang Z; Xu J; Bu XH Structural stabilization of a metal-organic framework for gas sorption investigation. Dalton Trans 2016, 45, 6830. [PubMed: 27028836]

(53). Duan X; Zhang Q; Cai J; Yang Y; Cui Y; He Y; Wu C; Krishna R; Chen B; Qian G. A new metal−organic framework with potential for adsorptive separation of methane from carbon dioxide, acetylene, ethylene, and ethane established by simulated breakthrough experiments. J. Mater. Chem. A 2014, 2, 2628.

(54). Xiang S; Zhou W; Zhang Z; Green MA; Liu Y; Chen B. Open Metal Sites within Isostructural Metal−Organic Frameworks for Differential Recognition of Acetylene and Extraordinarily High Acetylene Storage Capacity at Room Temperature. Angew. Chem., Int. Ed. 2010, 49, 4615.

(55). Duan J; Jin W; Krishna R. Natural gas purification using a porous coordination polymer with water and chemical stability. Inorg. Chem. 2015, 54, 4279. [PubMed: 25884592]

(56). Moreau F; da Silva I; Al Smail NH; Easun TL; Savage M; Godfrey HG; Parker SF; Manuel P; Yang S; Schroder M. Unravelling exceptional acetylene and carbon dioxide adsorption within a tetra-amide functionalized metal-organic framework. Nat. Commun. 2017, 8, 14085. [PubMed: 28176793]

(57). Pang J; Jiang F; Wu M; Liu C; Su K; Lu W; Yuan D; Hong M. A porous metal-organic framework with ultrahigh acetylene uptake capacity under ambient conditions. Nat. Commun. 2015, 6, 7575. [PubMed: 26123775]

(58). Xiang S; Zhou W; Gallegos JM; Liu Y; Chen B. Exceptionally High Acetylene Uptake in a Microporous Metal− Organic Framework with Open Metal Sites. J. Am. Chem. Soc. 2009, 131, 12415. [PubMed: 19705919]

(59). He Y; Krishna R; Chen B. Metal−organic frameworks with potential for energy-efficient adsorptive separation of light hydrocarbons. Energy Environ. Sci. 2012, 5, 9107.

(60). Giannozzi P; Baroni S; Bonini N; Calandra M; Car R; Cavazzoni C; Ceresoli D; Chiarotti GL; Cococcioni M; Dabo I; Dal Corso A; de Gironcoli S; Fabris S; Fratesi G; Gebauer R; Gerstmann U; Gougoussis C; Kokalj A; Lazzeri M; Martin-Samos L; Marzari N; Mauri F; Mazzarello R; Paolini S; Pasquarello A; Paulatto L; Sbraccia C; Scandolo S; Sclauzero G; Seitsonen AP; Smogunov A; Umari P; Wentzcovitch RM QUANTUM ESPRESSO: a modular and open-source software project for quantum simulations of materials. J. Phys.: Condens. Matter 2009, 21, 395502.

(61). Myers AL; Prausnitz JM Thermodynamics of mixed-gas adsorption. AIChE J. 1965, 11, 121.

(62). Krishna R. Screening metal−organic frameworks for mixture separations in fixed-bed adsorbers using a combined selectivity/capacity metric. RSC Adv. 2017, 7, 35724.

(63). Yao Z; Zhang Z; Liu L; Li Z; Zhou W; Zhao Y; Han Y; Chen B; Krishna R; Xiang S. Extraordinary Separation of Acetylene-Containing Mixtures with Microporous Metal-Organic Frameworks with Open O Donor Sites and Tunable Robustness through Control of the Helical Chain Secondary Building Units. Chem. - Eur. J. 2016, 22, 5676. [PubMed: 26934040]

(64). Stang PJ; Diederich F. Modern Acetylene Chemistry; VCH: New York, 1995.

NIST Author Manuscript

NIST Author Manuscript

NIST Author Manuscript

NIST Author Manuscript NIST Author Manuscript NIST Author Manuscript

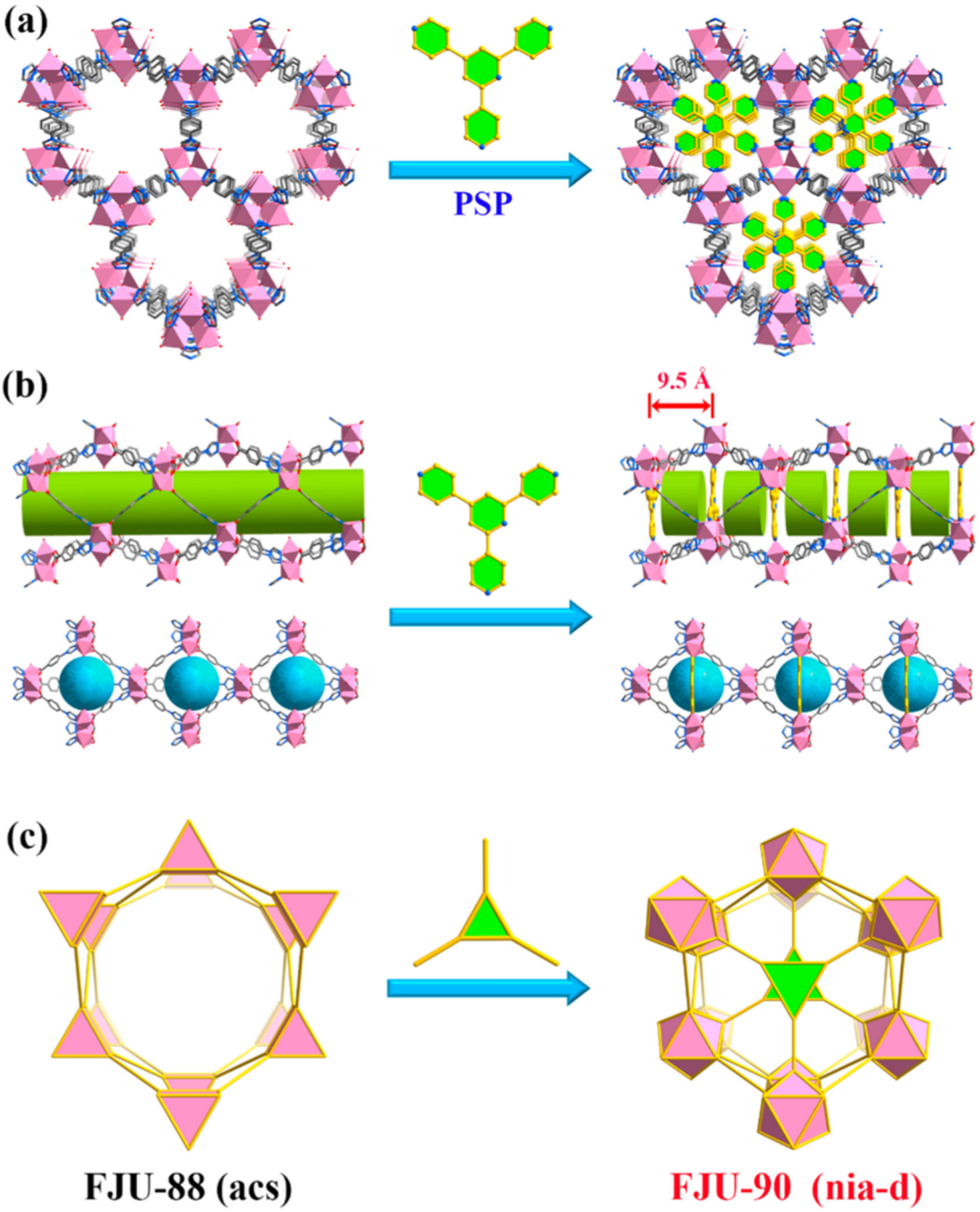

Figure 1.

Illustration of pore space partition (PSP) through symmetry- and size-matching-regulated ligand insertion. (a) Viewed along the crystallographic *c* axis of the cylindrical channel before and after partitioning. (b) Side view of the 1D cylindrical channel and trigonal bipyrimidal nanocages before and after partitioning. (c) Polyhedral drawing of the connected network in **FJU-88** and **FJU-90** before and after partitioning. Color code: Co, rose; O, red; N, light blue; C, gray or gold; Guest molecules and hydrogen atoms have been omitted for clarity.

NIST Author Manuscript

NIST Author Manuscript

NIST Author Manuscript

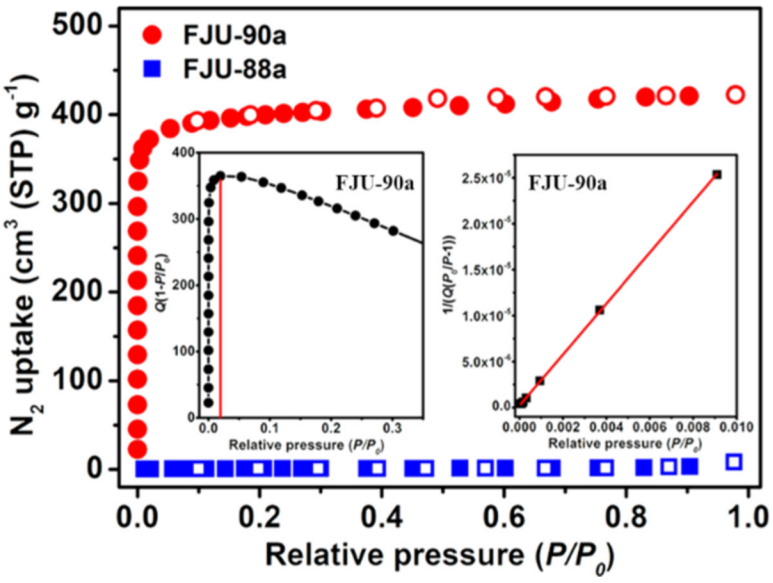

Figure 2.

N_2 sorption isotherms (at 77 K) for **FJU-88a** and **FJU-90a**. (Inset) BET plots for **FJU-90a**.

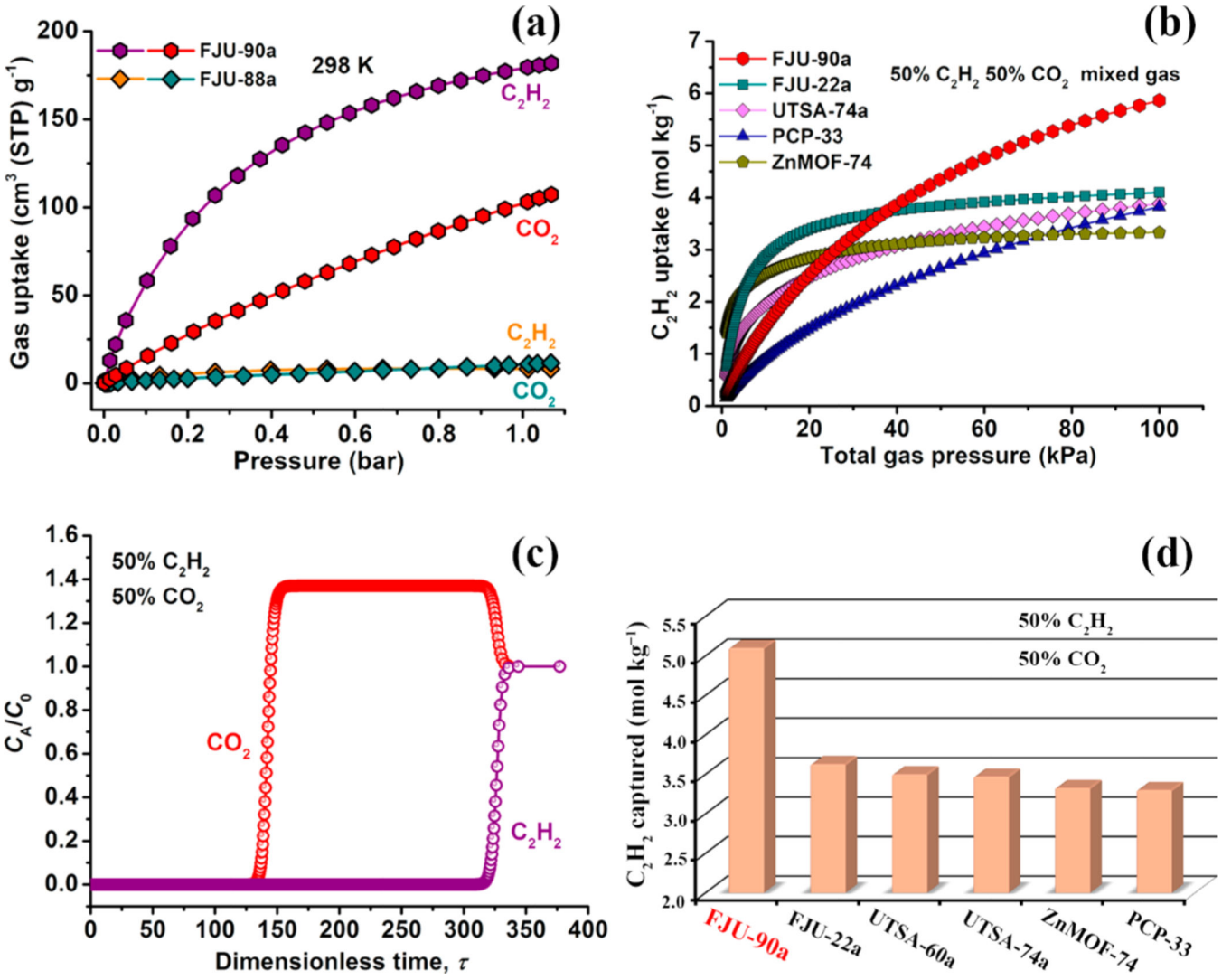

Figure 3.

(a) C_2H_2 and CO_2 single-component adsorption isotherms of **FJU-88a** and **FJU-90a** at 298 K under 1 bar. (b) Comparison of the IAST calculations of the C_2H_2 uptake of **FJU-90a** versus those of previously reported best-performing materials for equimolar C_2H_2/CO_2 mixtures. (c) Transient breakthrough simulations for the separation of equimolar C_2H_2/CO_2 mixtures using **FJU-90a** at 298 K, with a partial pressure of 50 kPa for each. (d) The C_2H_2 gravimetrically captured productivity of **FJU-90a** in comparison to that of the best-performing MOF materials reported to date and the productivity values of these MOFs were calculated from the simulated column breakthrough curves.

NIST Author Manuscript NIST Author Manuscript NIST Author Manuscript

NIST Author Manuscript
NIST Author Manuscript
NIST Author Manuscript

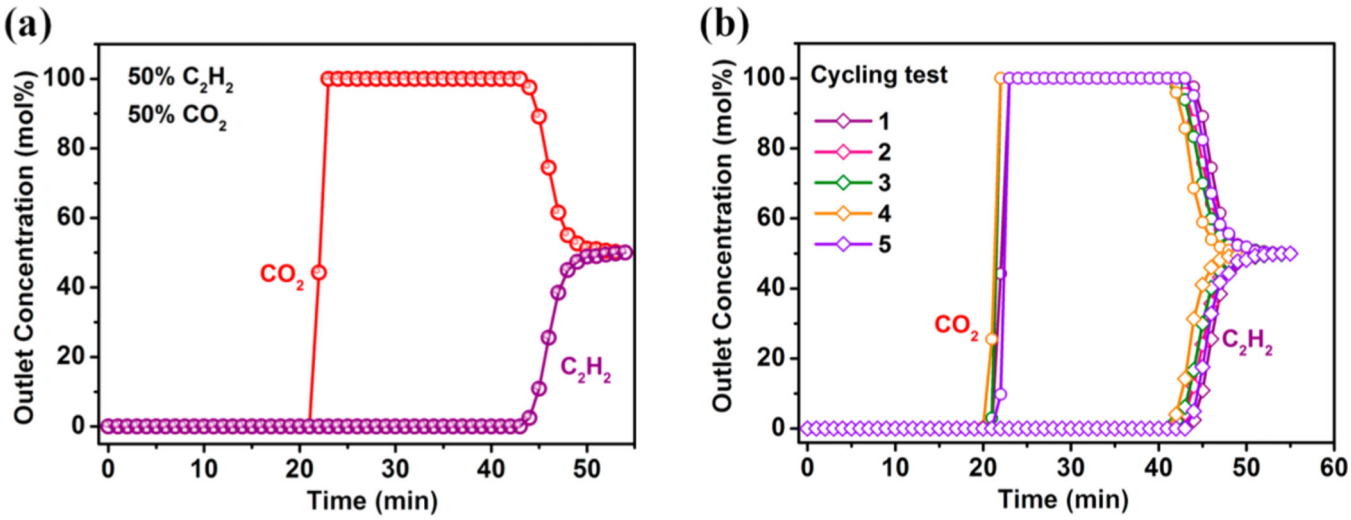

Figure 4.

Experimental breakthrough curves for (a) an equimolar C_2H_2/CO_2 mixture and (b) a cycling test of the equimolar C_2H_2/CO_2 mixture in a packed column with **FJU-90a** at 298 K and 1 bar.